

# Performance of hybrid turbulence models in OpenFOAM for numerical simulations of a confined backward-facing step flow at low Prandtl number

Wim Munters, Lilla Koloszar, and Philippe Planquart

Department of Environmental and Applied Fluid Dynamics, von Karman Institute for Fluid Dynamics, Waterlooosteenweg 72, 1640 Sint-Genesius-Rode, Belgium

**Abstract:** To date, numerical simulation of complex turbulent flows with separation remains challenging. On the one hand, turbulence models in Reynolds-averaged Navier-Stokes (RANS) equations struggle with correctly representing turbulent momentum transfer in such flows, whereas turbulence-resolving techniques such as large-eddy simulations (LES) carry high computational cost on the other hand. Alternatively, hybrid RANS–LES turbulence models promise to deliver scale-resolving accuracy at acceptable computational cost, yet their accuracy remains highly dependent on simulation setup and flow conditions. Here, we investigate hybrid turbulence models readily available in OpenFOAM, and benchmark their performance to Reynolds-averaged approaches and turbulence-resolving high-fidelity reference data for a confined backward-facing step flow at low Prandtl number and relatively low Reynolds number. Although temperature is generally well predicted by all considered setups, a comparison between RANS and LES shows that turbulence resolution can increase the accuracy for the considered flow case. Results show that scale-adaptive simulation techniques do not produce resolved turbulence and fail to outperform the baseline Reynolds-averaged simulations for the considered case. In contrast, detached-eddy variants do resolve turbulence in the separated shear layer, yet some configurations suffer from modeled-stress depletion due to late development of resolved turbulence. A grid coarsening study compares the degradation of accuracy for each approach, showcasing robustness of the standard RANS approach and the good performance of full LES even at surprisingly coarse resolutions. For each grid, the best-performing setup was either a RANS or an LES approach, but never a hybrid turbulence model setup. Finally, a Reynolds-number sensitivity is presented, indicating that resolved turbulence development is promoted at higher Reynolds numbers, thus leading to setups more amenable to hybrid turbulence models.

**Keywords:** hybrid turbulence modeling, large-eddy simulation, detached eddy simulation, scale-adaptive simulation, turbulent flows, OpenFOAM

## 1 Introduction

Simulating turbulent flows and heat transfer relevant for engineering applications remains a significant challenge to date, inspiring the development of a wide variety of simulation strategies. Direct numerical simulation (DNS) promises high accuracy but remains computationally far out of reach for any practical applications despite decades of evolution in computing infrastructure (Moin and Mahesh, 1998). Large-eddy simulations (LES) allow to relax the grid constraints of DNS by utilizing a sub-grid scale model for unresolved small-scale turbulence while explicitly resolving the energy-containing eddies (Sagaut, 2006). However, their applicability to engineering flows in complex geometries is still limited due to prohibitive computational costs in an industrial context. For example, current simulation roadmaps project DNS of a liquid-metal nuclear reactor pool to be feasible only after 2070, and we cannot expect to employ LES techniques on full pool geometries before 2040 (Roelofs et al., 2019). On the other side of the modeling spectrum, Reynolds-averaged Navier–Stokes (RANS) simulations can deliver timely numerical solutions by employing a model which parameterizes all effects of turbulence on resolved mean flow, thus eliminating the need for highly-refined turbulence-resolving simulation grids. Unfortunately, currently available turbulence models are typically only valid in one flow regime (e.g., natural, forced, or mixed convection) or geometry (e.g., jet, step, or wake flows), and perform poorly when faced with a multitude of flow regimes and configurations typical in engineering applications such as thermal hydraulics (Koloszar and Moreau, 2019).

This contrast between the prohibitive costs associated with full-scale high-fidelity DNS/LES and the affordable but limited-fidelity character of RANS has motivated the development of hybrid turbulence models, in which parts of the domain are treated according to DNS/LES techniques whereas others exhibit RANS behavior. Since the late 1990s, a large amount of different hybrid turbulence models have been developed based on various techniques for hybridization. Recent overviews of the general approach and state-of-the-art methods can be found, e.g., in Chaouat (2017) and Menter et al. (2021). These methods have historically been developed for aeronautical and ground transportation applications characterized by external flows with massive separation (see, e.g., Strelets, 2001; Slotnick et al., 2014), but they have found their way to various other applications as well, including internal low-Prandtl flows in nuclear thermal hydraulics applications (Bhushan et al., 2022). Although they have been used with success in many studies, several weaknesses have also become apparent over the years. For example, spurious switching to LES zones in insufficiently destabilized regions has been known to produce so-called modeled stress depletion (MSD), in which neither modeled (RANS) nor resolved (LES) turbulence produces sufficient mixing close to transition zones (Spalart, 2009). Furthermore, even

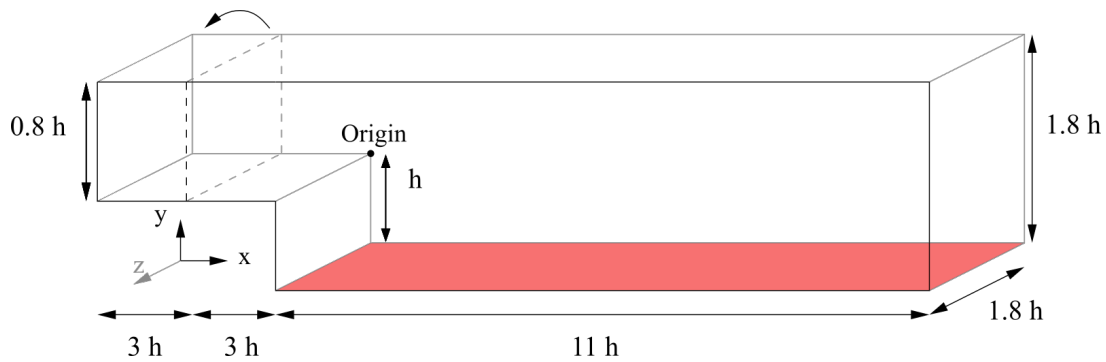


Fig. 1: Sketch of the BFS domain. The bottom wall colored in red is heated. Figure adapted from [Tiselj and Oder \(2019\)](#)

though their performance for external flows at high Reynolds numbers has been benchmarked to RANS and LES (see, e.g., [Freni et al., 2006](#); [Haase et al., 2009](#); [Ashton et al., 2016](#)), studies using hybrid turbulence models for internal flows at low to medium Reynolds numbers have been more scarce to date. Although such cases benefit from (partial) scale resolution, effects of viscosity and confinement have the potential to attenuate massive separation effects as observed in high-Reynolds external flows, which can be challenging for hybrid methods ([Spalart, 2009](#)).

In the current paper, we investigate hybrid turbulence models available in OpenFOAM, and benchmark their performance to fully Reynolds-averaged approaches, LES with partial scale resolution, and DNS resolving all turbulence scales. The scope of the study is deliberately limited to models readily available in OpenFOAM, justified by its status as one of the most widely used open-source computational fluid dynamics frameworks stemming from more than two decades of development ([Weller et al., 1998](#)). Hybrid models considered in the study are the unsteady-RANS-like scale-adaptive simulation model (SAS) and variants of the detached-eddy simulation model (DES). The benchmark is performed for a confined backward-facing step (BFS) flow at low Prandtl number and relatively low Reynolds number. The remainder of this paper is structured as follows. The BFS flow case is described in detail in Sect. 2, followed by the simulation methodology in Sect. 3. Next, simulation results of the considered hybrid turbulence models are compared to DNS and to baseline RANS and LES setups for a single grid in Sect. 4. Furthermore, sensitivity studies regarding grid resolution and Reynolds number are presented in Sect. 5. Finally, Sect. 6 summarizes the main conclusions and provides suggestions for further research.

## 2 Case description

We investigate an incompressible BFS flow, characterized by an inlet channel with a sudden step expansion. This expansion results in adverse pressure gradients and a large-scale separated shear layer (SSL) downstream of the step, which in turn causes anisotropy and recirculation. Although the geometry is simple, these flow phenomena justify the BFS as a standard test case for turbulence models (see, e.g., [Lien and Leschziner, 1994](#); [Probst et al., 2010](#); [Smirnov et al., 2018](#)).

We specifically focus on the reference BFS simulated with DNS as presented by [Oder et al. \(2019\)](#). The availability of such a reference database from DNS guarantees a high-fidelity numerical baseline without uncertainties related to turbulence modeling or experimental conditions. A sketch of the considered BFS geometry is presented in Fig. 1. Except for in- and outlet, all boundaries are solid walls, hence the BFS is confined. Upstream of the step, a recycling condition produces a fully developed turbulent channel flow with a bulk inlet velocity  $\langle u_{in} \rangle$ . The bottom wall past the step expansion is heated, where the wall temperature results from a conjugate heat transfer in the original DNS.

The flow is characterized by a relatively low Reynolds number  $Re = \langle u_{in} \rangle h / \nu = 6400$  and a low Prandtl number  $Pr = \nu / \alpha = 5 \times 10^{-3}$ , with  $\nu$  and  $\alpha$  the fluid kinematic viscosity and thermal diffusivity respectively. The reference flow dataset from [Oder et al. \(2019\)](#) is produced with the Nek5000 code <sup>1</sup> using the non-buoyant incompressible Navier–Stokes momentum and continuity equations for velocity  $\mathbf{u}$  and density-divided pressure  $p/\rho$ , along with a passive scalar transport equation for temperature  $\theta$  as

$$\frac{\partial}{\partial t} + \nabla \cdot = -\frac{1}{\rho} \nabla p + \frac{1}{Re} \nabla^2, \quad (1)$$

$$\nabla \cdot = 0, \quad (2)$$

$$\frac{\partial \theta}{\partial t} + \nabla \cdot \theta = \frac{1}{Pr Re} \nabla^2 \theta. \quad (3)$$

## 3 Simulation methodology

Simulations are compared for different turbulence models in OpenFOAM. This study is limited to out-of-the-box configurations readily available in the v2012 release.<sup>2</sup> The numerical setup, including the simulation grid, boundary conditions and OpenFOAM solvers, is described in Sect. 3.1. Next, the different turbulence models considered in this study are detailed in Sect. 3.2.

<sup>1</sup><http://nek5000.mcs.anl.gov>

<sup>2</sup>Available at: <https://develop.openfoam.com/Development/openfoam/-/releases/OpenFOAM-v2012>

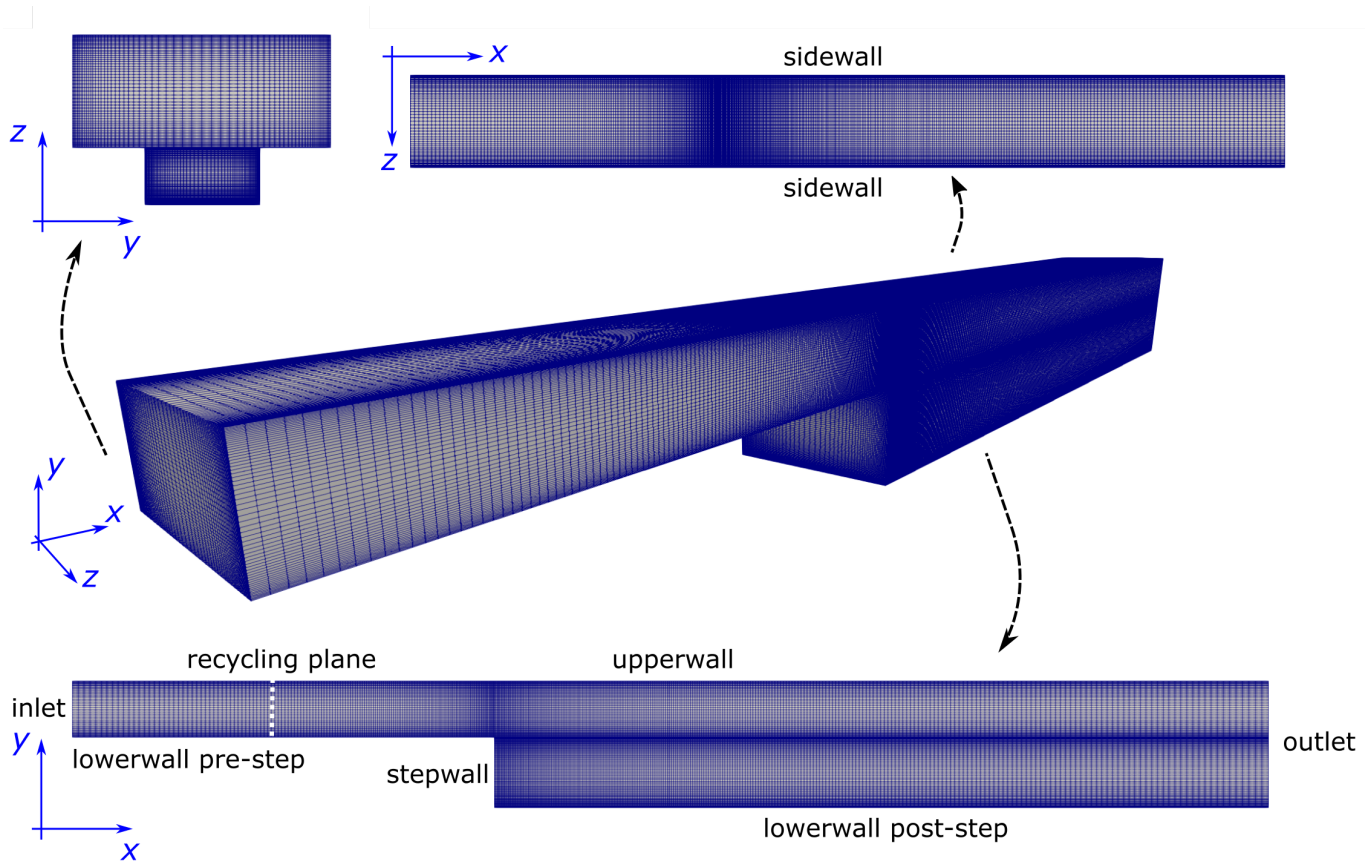


Fig. 2: Overview of the baseline simulation grid with 3.7 million grid cells.

### 3.1 Numerical setup

Simulations are performed on an identical baseline simulation grid illustrated in Fig. 2. The grid is created with the `blockMesh` tool, and is sufficiently refined to support all turbulence modeling strategies considered here. The wall resolution is chosen to resolve the viscous sublayers such that  $y^+ = u_\tau y / \nu \approx 1$  averaged over solid surfaces, with  $u_\tau$  the local friction velocity,  $y$  the first cell-center height off the wall, and  $\nu$  the kinematic viscosity. The overall grid is further built with uniform stretching using the `simpleGrading` tool, such that resolution of large eddies remains supported throughout the domain, resulting in a grid of about 3.7 million cells. Initial tests showed that this grid supports LES in which about 94% of the turbulence in the domain is resolved, whereas the remaining 6% is accounted for by the sub-grid scale model.

Boundary conditions are summarized in Tab. 1. Matching the DNS reference setup, the inlet applies a ‘mapped condition’ which introduces the solution at the recycling plane back at the inlet, resulting in a periodic channel flow between inlet and recycling plane. Walls are treated with no-slip conditions (no wall functions are used), zero-gradient pressure, and appropriate fixed-value conditions for turbulence model quantities<sup>3</sup>. At the outlet, a reference pressure value is fixed, whereas other flow quantities are subject to zero-gradient and zero-backflow conditions. For temperature, all domain boundaries except the lower post-step wall are treated as adiabatic. Instead of explicitly modeling the conjugate heat transfer as in [Oder et al. \(2019\)](#), we map the DNS time-averaged temperature (which ranges between 24.6 and 38.9 dimensionless units) directly as a fixed-value thermal boundary condition.

Steady cases are solved using the `simpleFoam` solver, whereas the  `pisoFoam`  solver is used for transient simulations. Unsteady simulations are initialized using a steady RANS solution. Subsequently, simulations are advanced in time until a statistically stationary state is observed, after which statistical sampling is performed over a time horizon of about 50 domain flow-throughs.

### 3.2 Turbulence modeling

To mitigate the excessive computational cost of resolving the full velocity field down to Kolmogorov scales as in DNS, this field is either represented by a time- or ensemble average in RANS, or by a coarse-grained filtered  $\tilde{\cdot}$  in LES.<sup>4</sup> This procedure introduces unclosed turbulent stresses in the governing equations (1) - (3) representing unresolved momentum and thermal transport that have to be closed by an appropriate turbulence or sub-grid scale model. In the current work, models of eddy-viscosity type are used, which relate unresolved momentum stress to the resolved rate-of-strain tensor through the use of an eddy viscosity  $\nu_t$ . In turn, unresolved thermal diffusivity is related to  $\nu_t$  through the Reynolds analogy, with a turbulent Prandtl number  $Pr_t = 2$  for RANS-type models ([Bartosiewicz and Duponcheel, 2019](#)) and a sub-grid Prandtl number  $Pr_t = 0.4$  for LES-type models ([Sagaut, 2006](#)). Within the current paper, six different turbulence models are considered, consisting of baseline RANS and LES setups, an

<sup>3</sup>Note that the `omegaWallFunction` in OpenFOAM is a fixed-value condition rather than an actual wall function

<sup>4</sup>In the remainder of this manuscript, the tilde notation is omitted and overlines indicate time-averaged variables.

Tab. 1: Overview of boundary conditions for all variables along with the associated OpenFOAM keyword. Note that the variable  $\omega$  is not used in LES.

		inlet	outlet	lowerwall post-step	other walls
Velocity	$\mathbf{u}$	Recycling (mapped)	$\partial \mathbf{u} / \partial n = 0$ or $\mathbf{u} \cdot \mathbf{n} = 0$ (inletOutlet)	$\mathbf{u} = 0$ (noSlip)	$\mathbf{u} = 0$ (noSlip)
Temperature	$\theta$	Fixed: $\theta = 0$ (zeroGradient)	Adiabatic: $\partial_n \theta = 0$ (zeroGradient)	Mapped from DNS (fixedValue)	Adiabatic: $\partial_n \theta = 0$ (zeroGradient)
Pressure	$p$	$\partial_n p = 0$ (zeroGradient)	Fixed: $p = 0$ (fixedValue)	$\partial_n p = 0$ (zeroGradient)	$\partial_n p = 0$ (zeroGradient)
TKE	$k$	Recycling (mapped)	$\partial_n k = 0$ (zeroGradient)	$k = 0$ (fixedValue)	$k = 0$ (fixedValue)
TKE dissipation	$\omega$	Recycling (mapped)	$\partial_n \omega = 0$ (zeroGradient)	$\omega = 6\nu / (0.075y_1^2)$ (omegaWallFunction)	$\omega = 6\nu / (0.075y_1^2)$ (omegaWallFunction)

Tab. 2: Overview of simulation cases.

Case	Resolution of large eddies	Turbulence model	Modeled turbulence length scale
RANS	None	$k - \omega$ SST	$d_{SST} = k^{0.5} / (0.09\omega)$
LES	Everywhere (down to grid scale $\Delta$ )	$k$ (dynamic)	$d_{LES} = C_{LES}\Delta$
SAS	Hybrid: based on solution	$k - \omega$ SST SAS	$d_{SAS} = d_{SST} / d_{vK}$
DES	Hybrid: based on solution + grid	$k - \omega$ SST DES	$d_{DES} = \min(d_{SST}, d_{LES})$
DDES	Hybrid: DES + boundary-layer shielding	$k - \omega$ SST DDES	$d_{DDES} \approx d_{SST}$ (close to walls) $\approx d_{DES}$ (away from walls)
IDDES	Hybrid: DDES + WMLES features	$k - \omega$ SST IDDES	$d_{IDDES} \approx d_{SST}$ (close to walls) $\approx d_{DES}$ (away from walls) (+ log-layer modifications)

extended unsteady RANS hybrid model, and three RANS/LES-based hybrid turbulence models. Note that all turbulence models mentioned below are readily available in OpenFOAM v2012 and are used in their default configuration. Simulation cases for all six turbulence models considered here are summarized in Tab. 2.

Baseline RANS and LES are performed as lower and upper limits of expected attainable performance by the hybrid models. The RANS uses the  $k - \omega$  SST turbulence model (Menter et al., 2003), whereas the LES uses a high-fidelity dynamic  $k$  sub-grid scale model (Kim and Menon, 1995). Both models rely on a prognostic equation for the modeled turbulent kinetic energy  $k$ . This prognostic equation contains a destruction term which is inversely proportional to a modeled turbulence length scale  $d$ . In this way, smaller values for  $d$  result in a reduction of modeled  $k$ , in turn yielding lower eddy viscosity  $\nu_t$ . The main difference in governing equations of unsteady RANS and LES lies in how  $d$  is defined. In RANS it depends solely on the solution as, e.g.,

$$d_{SST} = k^{0.5} / (0.09\omega) \quad (4)$$

for the  $k - \omega$  SST model. For LES on the other hand, in line with the implied filtering of variables at the grid scale, the modeled turbulence length scale is directly related to the local grid resolution  $\Delta$  as

$$d_{LES} = C_{LES}\Delta \quad (5)$$

instead, with  $C_{LES}$  a constant in the order of 0.1 (dependent on local flow variables in dynamic formulations). In this way, on finer LES grids the foregoing  $\nu_t$  reduction destabilizes the numerical solution to facilitate resolution of large eddies.

A first hybrid setup consists of the  $k - \omega$  SST SAS turbulence model (Egorov and Menter, 2008). The SAS methodology can be viewed as an extension to unsteady RANS in the sense that turbulence modeling is based solely on physical length scales derived from the solution flow fields. In addition to the standard  $k - \omega$  SST length scale  $d_{SST}$ , the underlying turbulence model in SAS is provided with a second independent von-Kármán length scale  $d_{vK}$  based on the ratio of first and second-order velocity gradients. This allows to automatically reduce  $\nu_t$  in regions of strong shear and inherent instability without relying explicitly on grid or time step parameters, thus promoting eddy resolution based solely on the properties of the numerical solution.

In contrast, the other three hybrid setups considered in this work lean more towards an LES approach, in which also the grid resolution  $\Delta$  plays a direct role in the turbulence model in addition to physical properties in the numerical solution. More specifically, three variants of DES methods are considered. Firstly, we consider the  $k - \omega$  SST DES developed by Strelets (2001), which defines a length scale

$$d_{DES} = \min(d_{SST}, C_{DES}\Delta). \quad (6)$$

Note that this results in DES adhering to the smallest of either the RANS or the LES length scale formulation.<sup>5</sup> Eq. (6) implies that, if the local length scale of modeled turbulence exceeds  $C_{DES}\Delta$ , it will no longer be accounted for in the  $k - \omega$  SST model, since the local grid resolution should suffice in resolving scales larger than this threshold. Mathematically, this results in a reduced eddy viscosity  $\nu_t$ , which facilitates destabilization of the numerical solution to resolve turbulence in LES mode.

Secondly, the  $k - \omega$  SST Delayed DES (DDES) formulation proposed by Gritskevich et al. (2012) is used. DDES defines a shielding function  $f_d$ , which is used to avoid spurious grid-induced transition to scale-resolving regimes in regions characterized by significant grid refinement but insufficiently strong flow instabilities to rapidly produce resolved turbulence such as attached boundary layers. This problem is known to severely impact accuracy in standard DES, therefore motivating to define the length scale in DDES as

$$d_{DDES} = d_{SST} - f_d \max(d_{SST} - C_{DES}\Delta), \quad (7)$$

with  $f_d \approx 0$  close to walls, hence  $d_{DDES} \approx d_{SST}$  and  $f_d \approx 1$  away from them, resulting in  $d_{DDES} \approx d_{DES}$ . Third, the  $k - \omega$  SST Improved DDES model (IDDES) is employed (Gritskevich et al., 2012), which features slight modifications of the DDES length scale to avoid so-called log layer mismatch close to solid boundaries and make it more amenable wall-modeled LES (WMLES) operation.

## 4 Results on baseline grid

In this section, we show the performance of the different turbulence models and compare them to each other and to the reference DNS data, with specific focus on the hybrid models. Firstly, we set the baseline performance by comparing the full RANS and LES approaches in Sect. 4.1 as the expected lowest and highest fidelity turbulence models respectively. Next, we discuss the behavior of the different hybrid setups in Sect. 4.2. Finally, we discuss the overall performance of all methods quantitatively in Sect. 4.3.

### 4.1 Setting the bar: performance of RANS and LES

**Qualitative flow field description** A qualitative view of the flow and temperature fields in LES and RANS is shown in Fig. 3. It can be seen that, while the RANS streamwise velocity is smooth and time-averaged by construction (a), the LES counterpart (d) features turbulent structures throughout the domain. Looking at the time-averaged vertical velocities in (b) and (e), the 3D structure of the fields is very different, especially in the downstream vicinity of the step. In contrast, differences in the mean temperature between RANS (c) and LES (f) are much more subtle. This can be attributed to the geometry and boundary conditions of the temperature field, but more importantly to the low Prandtl number  $Pr = 5 \times 10^{-3}$ , resulting in a temperature distribution that is governed by molecular diffusion rather than turbulent mixing. In Fig. 4, the time-averaged LES field (b) can be compared to the inherently time-averaged RANS field (a). The main qualitative difference that can be observed from these plots is the increased coherence of a jet-type flow at the top part of the outlet in RANS, whereas this jet is significantly more diffused in LES. Furthermore, close observation of the streamlines shows a different structure of the recirculation bubble in both cases, i.e., a very flat and long bubble in RANS versus an inclined shorter bubble in LES.

**Midplane profiles** Profiles of flow quantities along the domain midplane are compared to DNS data in Fig. 5. For the horizontal velocity  $\bar{u}$  (a), it can be seen that the turbulent channel profiles from DNS are matched well by both RANS and LES. However, downstream of the step, RANS shows significant deviations from the DNS whereas LES retains a good match throughout the domain. More specifically, the backflow velocity in the separation bubble close to the step ( $1 \leq x/h \leq 3$ ) is significantly underpredicted by RANS, whereas the flow velocity in the top right part of the domain is overpredicted ( $3 \leq x/h \leq 11, 0 \leq y/h \leq 0.8$ ). Turning to the vertical velocity  $\bar{v}$  in panel (b), it is seen that the LES achieves an acceptable match with the DNS data. Even though the velocity is lower than the DNS data for  $4 \leq x/h \leq 10, -1 \leq y/h \leq 0$ , the overall shape of the profile is retained. In contrast, RANS only matches the DNS profile at  $x/h = 2$ , while the S-shaped profiles observed in DNS and LES are not found at all in the RANS solution. In addition to the mean-flow quantities discussed above, Fig. 5c) contains profiles of the resolved and modeled time-averaged turbulent kinetic energy  $\bar{k}$ . LES achieves a good match with DNS, although slight overpredictions are observed for  $2 \leq x/h \leq 4, -1 \leq y \leq 0$ . Furthermore, the LES seems highly resolved, i.e., sub-grid modeled components are much smaller than the resolved components. Regarding the modeled turbulence in RANS, we see the largest discrepancies with DNS are observed in the SSL close to the step, where turbulence is generally underpredicted. Downstream, the match with DNS is improved, although it remains worse than the LES. Midplane profiles for time-averaged temperature  $\bar{\theta}$  are shown in Fig. 6. It is clearly shown that, despite the observed differences in the velocity profiles above, there is a very good match with DNS temperature profiles for both RANS and LES, apart from a minor deviation in the RANS temperature profiles at  $x/h = 2$ . As mentioned above, this is mainly caused by the low Prandtl number, resulting in a strongly viscosity-dominated temperature transport.

**Summary** We conclude here that LES is able to match the DNS data throughout the entire domain, whereas RANS exhibits significant discrepancies in the velocity field downstream of the step. This observation is in line with the motivation for using hybrid RANS/LES turbulence models, as large-eddy scale resolution in the downstream zone could hence be capable of increasing overall accuracy.

<sup>5</sup>In practice,  $C_{DES}$  slightly differs from  $C_{LES}$  to accommodate different zones in the  $k - \omega$  SST model.

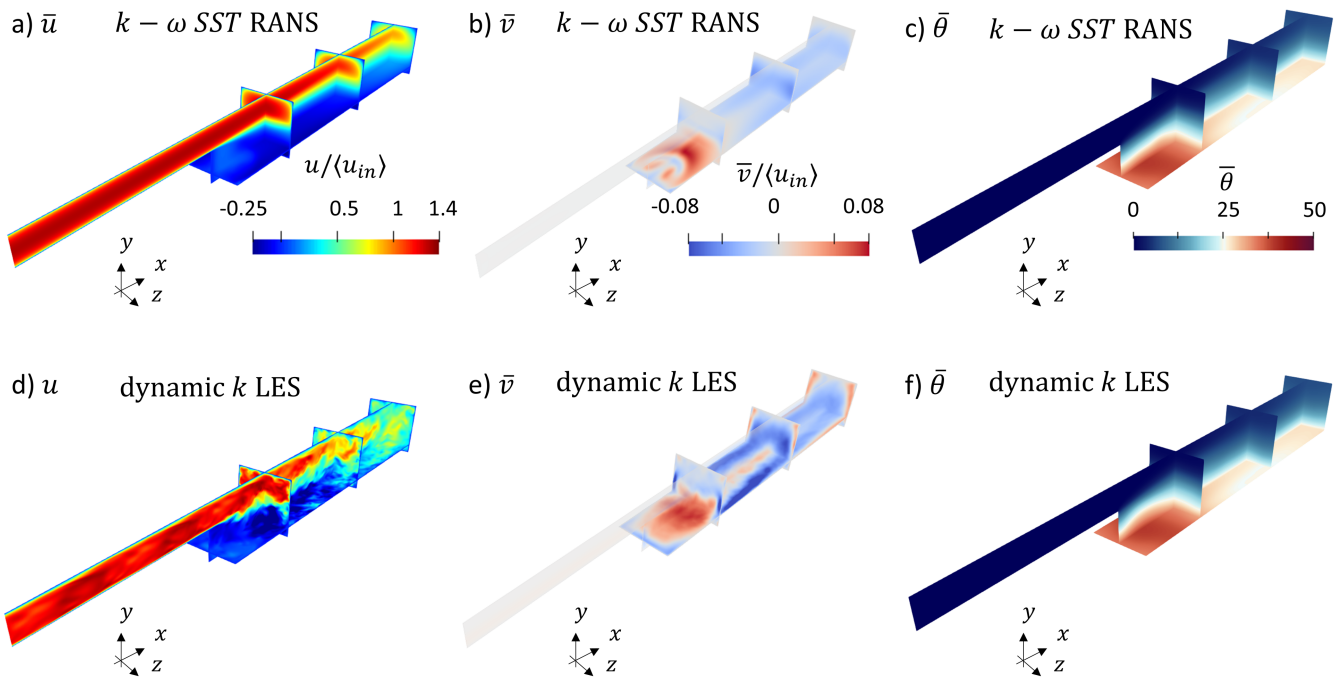


Fig. 3: Flow field visualization for RANS (top, a, b, c) and LES (bottom, d, e, f) of streamwise velocity  $u$  (left, a, d) and vertical velocity  $v$  (middle, b, e), and temperature (right, c, f). All except (d) illustrate time-averaged quantities.

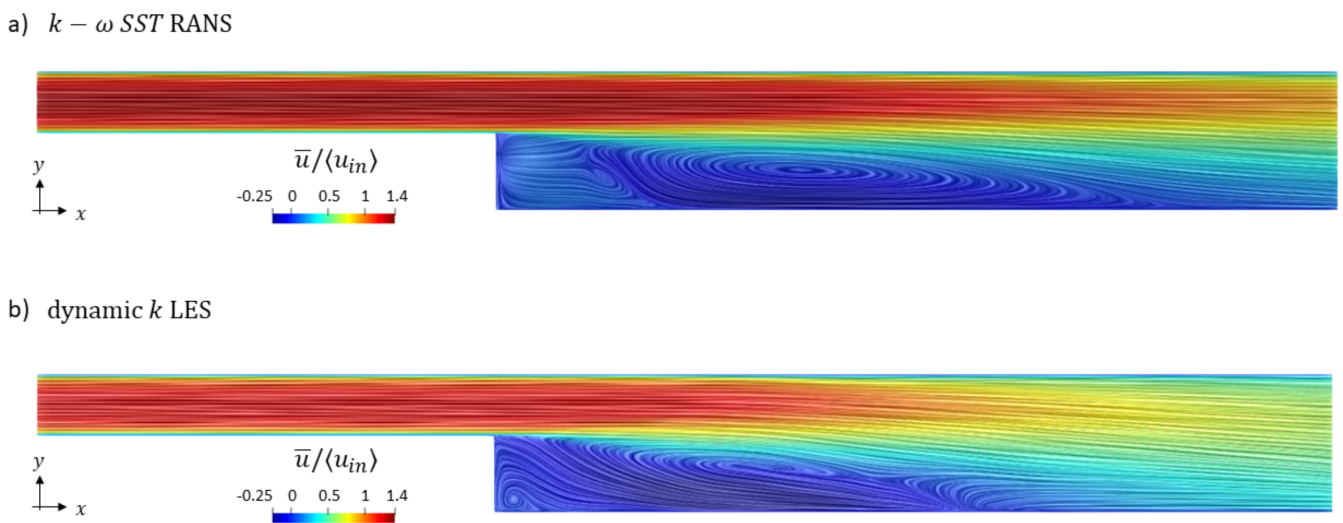


Fig. 4: Mean streamwise velocity  $\bar{u}$  of RANS (a) and LES (b) with in-plane streamlines.

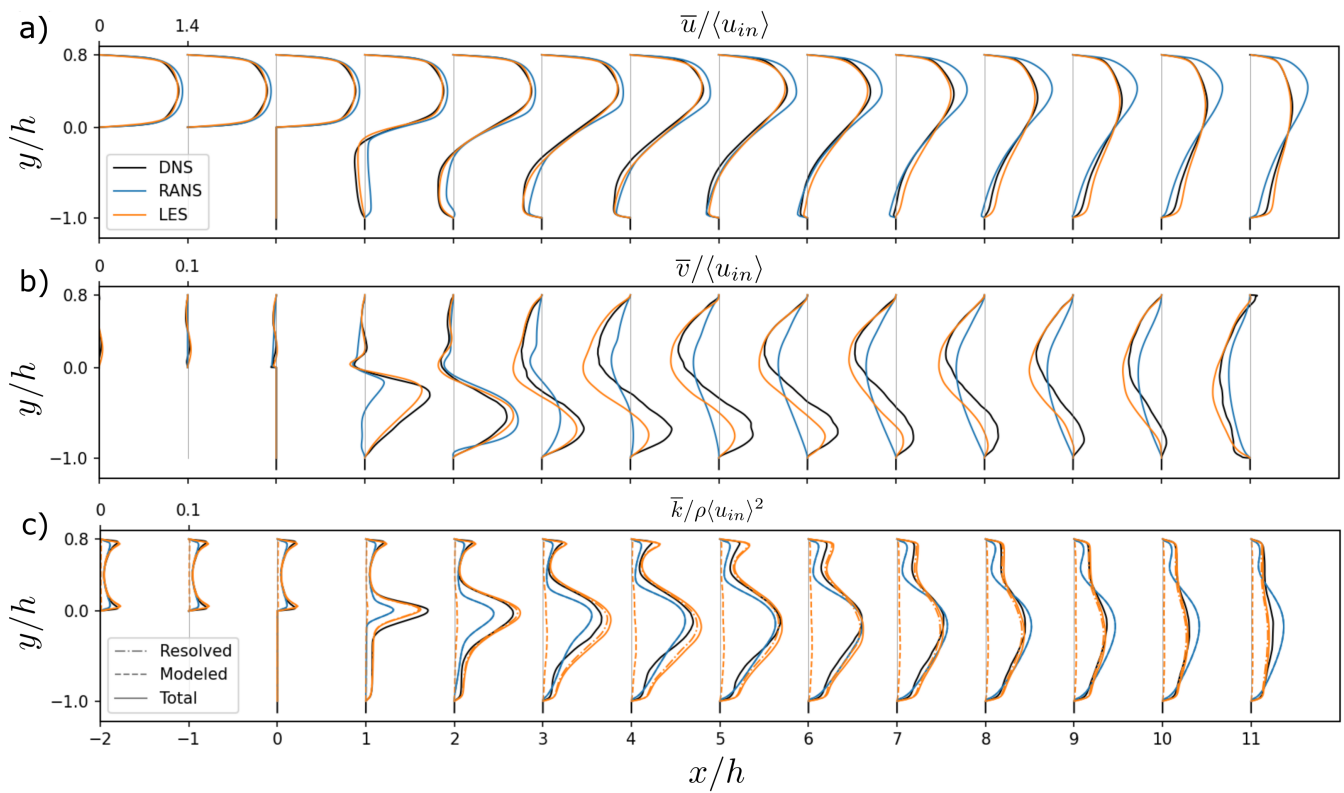


Fig. 5: Profiles along midplane for DNS, RANS, and LES. (a) Streamwise velocity component  $\bar{u}$ . (b) Vertical velocity component  $\bar{v}$ . (c) Turbulent kinetic energy  $\bar{k}$ . Dashed, dot-dashed, and full lines indicate modeled, resolved and total (modeled + resolved) components. (Modeled and resolved components in DNS and RANS respectively are zero by definition and not further shown).

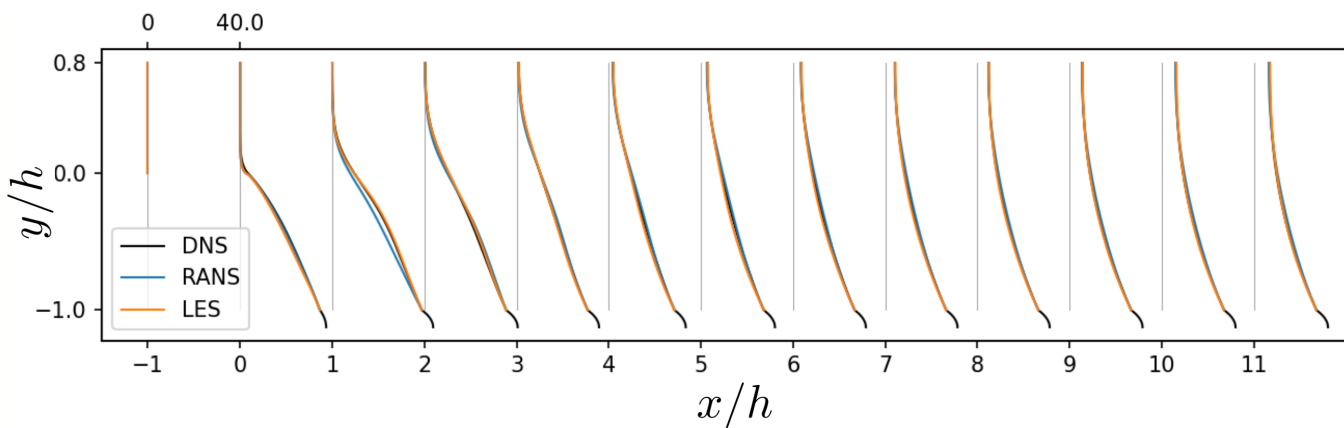


Fig. 6: Profiles of time-averaged temperature  $\bar{\theta}$  for DNS, RANS, and LES.

## 4.2 Behavior of hybrid methods

The behavior of the hybrid turbulence models considered in this paper are discussed below. Firstly, the URANS-like SAS technique is addressed in Sect. 4.2.1. Next, the DES are shown in Sect. 4.2.2. Finally, Sect. 4.2.3 and 4.2.4 discuss the delayed and improved-delayed DES variants, DDES and IDDES.

### 4.2.1 Scale-Adaptive Simulations (SAS)

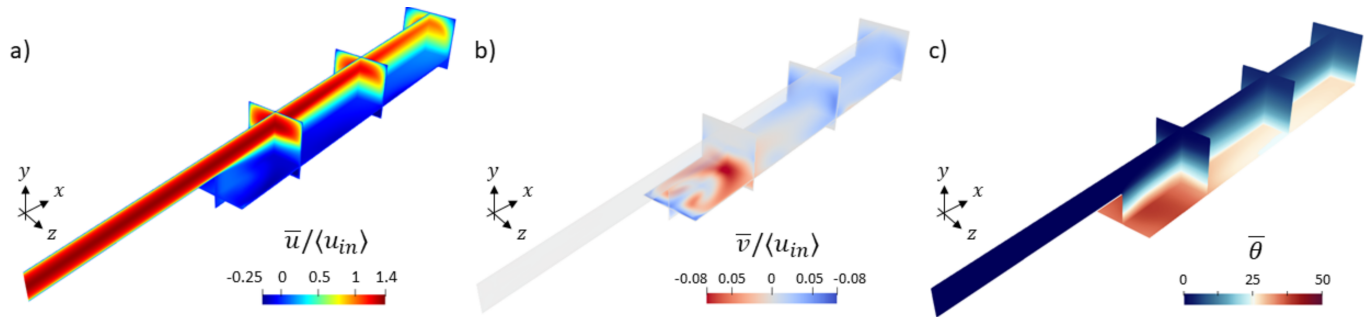


Fig. 7: Flow field visualization for SAS. a) Streamwise velocity snapshot  $u$ . b) Time-averaged vertical velocity  $\bar{v}$ . c) Time-averaged temperature  $\bar{\theta}$ .

**Qualitative flow field description** Fig. 7 shows a snapshot of streamwise velocity (a) as well as the time-averaged vertical velocity (b) and temperature. A first observation is that the streamwise velocity snapshot is free of any resolved turbulence fluctuations. Next, the vertical velocity in the case of SAS exhibits a similar structure as that in RANS shown in Fig. 3b), which was discussed to match poorly with the DNS reference. Furthermore, temperature fields show qualitative similarities to those of RANS and LES shown before. Finally, the structure of the recirculation bubble as shown in Fig. 8 resembles the one observed in the RANS (Fig. 4), even though the separation zone extends even more downstream in the current SAS.

**Summary** Also upon investigation of the midplane profiles, which are not presented here for brevity, the SAS was found to be very similar (velocities) and virtually identical (temperature) to RANS. Even though the simulation grid should support scale resolution, as it is a proper LES mesh, no resolved turbulence was observed in the SAS. Summarizing, in the current setup, SAS fails to differentiate itself from a standard RANS and hence does not improve model fidelity.

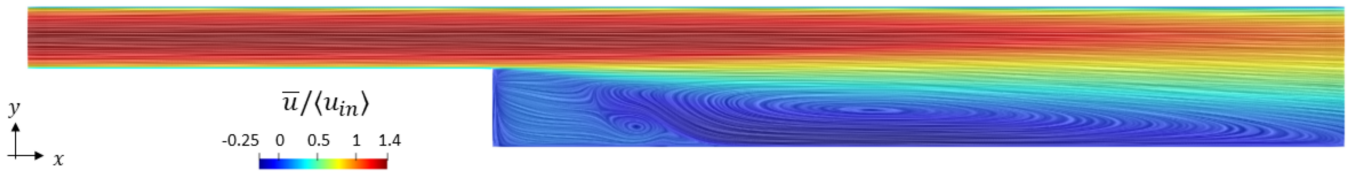


Fig. 8: Time-averaged streamwise velocity  $\bar{u}$  of SAS with in-plane streamlines.

### 4.2.2 Detached Eddy Simulations (DES)

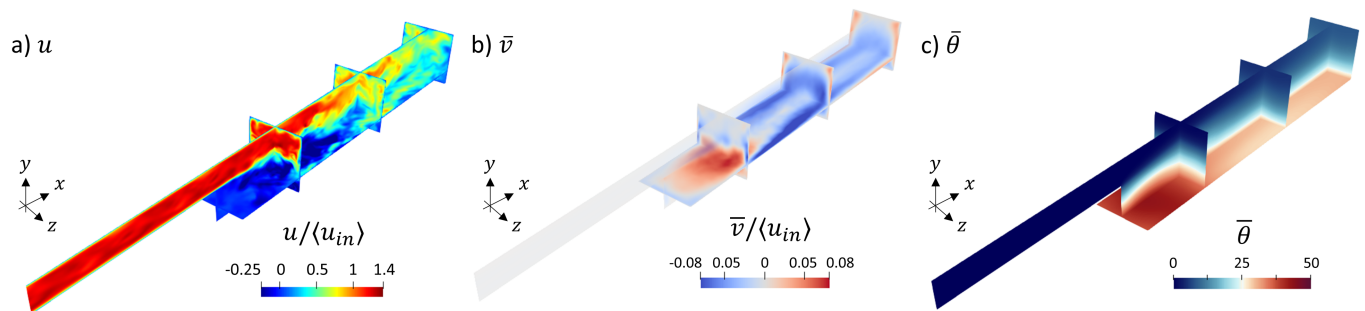


Fig. 9: Flow field visualization for DES. a) Streamwise velocity snapshot  $u$ . b) Time-averaged vertical velocity  $\bar{v}$ . c) Time-averaged temperature  $\bar{\theta}$ .

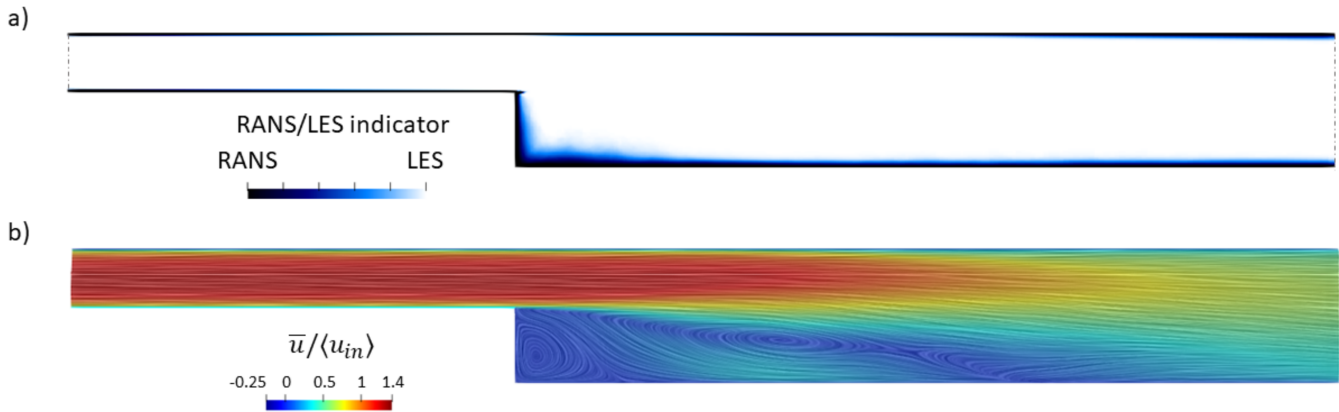


Fig. 10: Midplane side view of DES simulation. (a) Time-averaged RANS / LES indicator function. White is always LES, black is always RANS, mix is sometimes LES, sometimes RANS. (b) Time-average streamwise velocity  $\bar{u}$ , including in-plane streamlines.

**Qualitative flow field description** As shown in Fig. 9, the DES qualitatively behaves much like the LES from Fig. 3, including a domain filled with turbulent fluctuations for the snapshot and a similar structure in vertical velocity and temperature as observed in the LES. Fig. 10a) illustrates the time-averaged RANS / LES indicator function, which is defined based on the modeled turbulence lengthscale (see Tab. 2) with the `DESModelRegions` function in OpenFOAM. It can be seen that the majority of the midplane is consistently treated as LES, while regions very close to the wall turn to a RANS approach. Only the region closely downstream of the step exhibits some switching between RANS and LES. Apart from the latter, the DES thus behaves very similar to a WMLES. The recirculation structure highlighted in Figure 10b) is again similar to the one observed in LES.

**Midplane profiles** Fig. 11 compares the midplane profiles of DES to DNS and LES (along with the DDES and IDDES variants, which are discussed in sections below). Again, a strong similarity between LES and DES is observed, except very close to the step, where DES underpredicts both the vertical velocity  $\bar{v}$  and the turbulence kinetic energy  $\bar{k}$ , potentially related to the RANS behavior of this region. Temperature profiles in Fig. 12 again show the resemblance between DES and LES results.

**Summary** Results show that DES behaves like a (WM)LES for the current setup on a LES-capable simulation grid. The sections below focus on extensions of DES, which were specifically designed to delay the transition to LES in wall-bounded flow regions such as the inlet channel (DDES), or have special amenities for proper WMLES (IDDES).

#### 4.2.3 Delayed Detached Eddy Simulations (DDES)

**Qualitative flow field description** DDES has been originally designed to avoid the transition to LES mode in wall-attached boundary layers such as the inlet channel region of the current BFS domain (Gritskevich et al., 2012). Interestingly, Fig. 13a) indicates that this channel region does not contain any fluctuations, and that the onset of scale resolution is delayed to the far downstream region of the SSL. The vertical velocity structure in Fig. 13b) is completely different than for any of the preceding cases, with a strong downward component towards the end of the domain, which is potentially related to the onset of resolved turbulence and the influence of the outlet boundary condition. Qualitatively, the temperature field is again similar as for other cases as shown in Fig. 13c). The RANS / LES indicator function shown in Fig. 14 reveals a hybrid domain division into a RANS zone in the upstream channel and top-wall attached boundary layer, whereas the SSL is treated with LES. This domain partitioning is highly desirable, since RANS was shown to work well in such regions and is expected to allow significant grid coarsening, whereas LES should enhance fidelity in the SSL. However, when comparing the vertical velocity structure in Fig. 13b), we see that neither of the expected structures observed before in RANS or LES is attained.

**Midplane profiles** Further looking at midplane profiles in Fig. 11, DDES produces a poor match with DNS / LES. The expected recirculation zone ( $0 \leq x/h \leq 6, -1 \leq y/h \leq 0$ ) appears to be almost stagnant with no recirculation predicted by DDES. Furthermore, the vertical velocity is very much underpredicted in this zone, which seems to be compensated by far too large negative vertical velocities in the outlet zone ( $x/h \geq 8$ ). Focusing on turbulence profiles in Fig. 11c), it becomes clear that DDES is suffering from severe MSD in the expected recirculation zone. Even though the model has turned to an LES formulation here (thus without support of a RANS turbulence model), this zone is turbulence-deficient without any resolved scales to take up the turbulent mixing effects. Finally, the different flow field structure even results in discrepancies in temperature profiles as shown Fig. 12.

**Summary** The DDES achieves a poor match with DNS or LES, and clearly stands out from the other DES variants, both in terms of accuracy and RANS / LES domain partitioning. The root cause of poor performance is MSD due to late production of resolved turbulence far downstream of the separation point. We hypothesize that this delayed transition is related to the relatively low Reynolds number of the case under consideration. This is further addressed in the DDES Reynolds-number sensitivity study in Sect. 5.2.

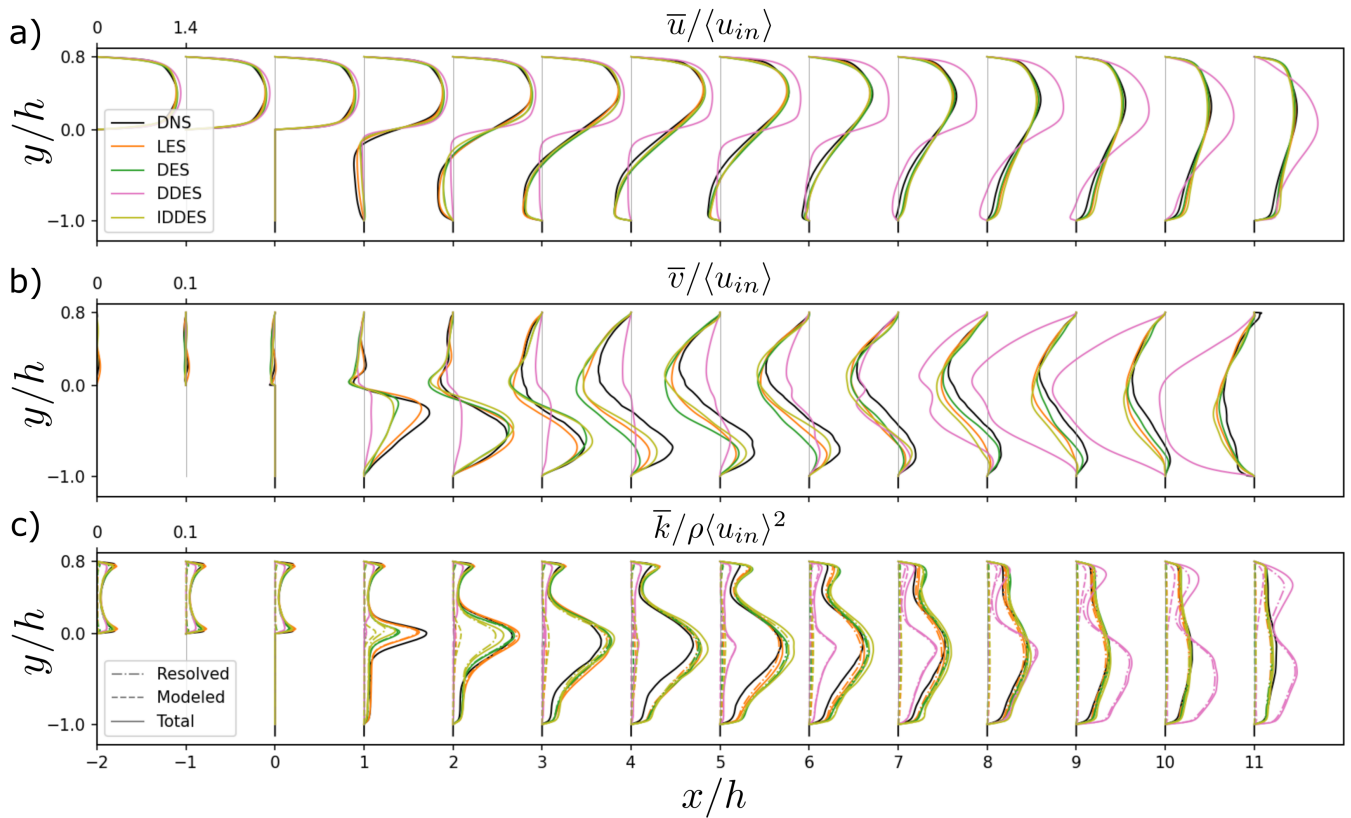


Fig. 11: Profiles along midplane for DNS, LES, and DES variants. (a) Streamwise velocity component  $\bar{u}$ . (b) Vertical velocity component  $\bar{v}$ . Turbulent kinetic energy  $\bar{k}$ . (c) Dashed, dot-dashed, and full lines indicate modeled, resolved and total (modeled + resolved) components.

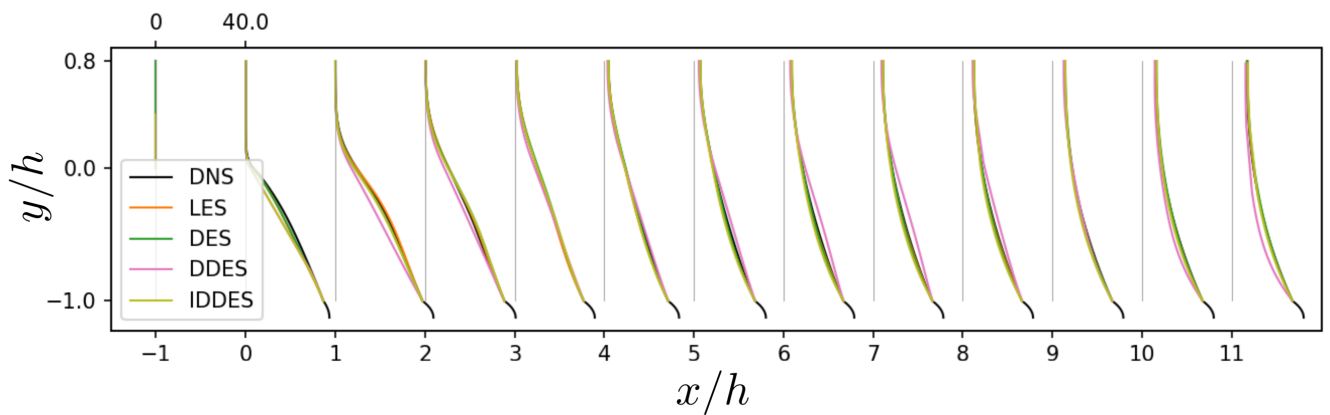


Fig. 12: Time-averaged temperature profiles along midplane for DNS, LES, and DES variants.

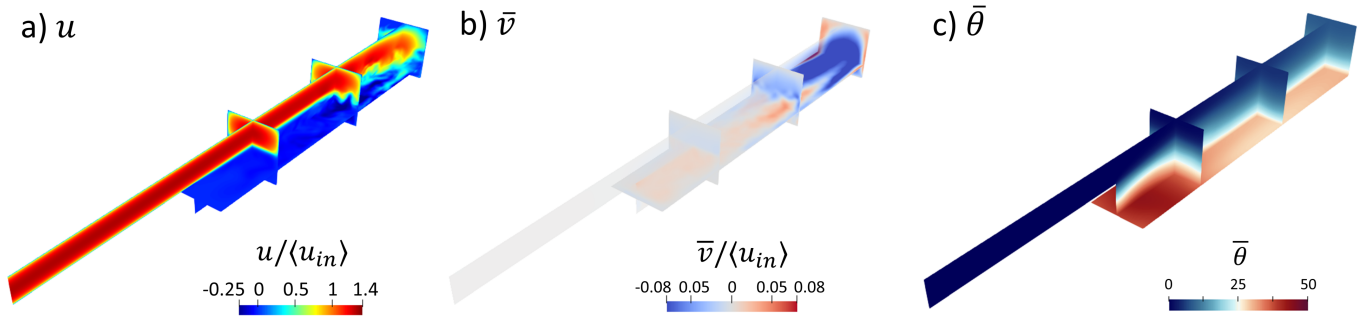


Fig. 13: Flow field visualization for DDES. a) Streamwise velocity snapshot  $u$ . b) Time-averaged vertical velocity  $\bar{v}$ . c) Time-averaged temperature  $\bar{\theta}$ .

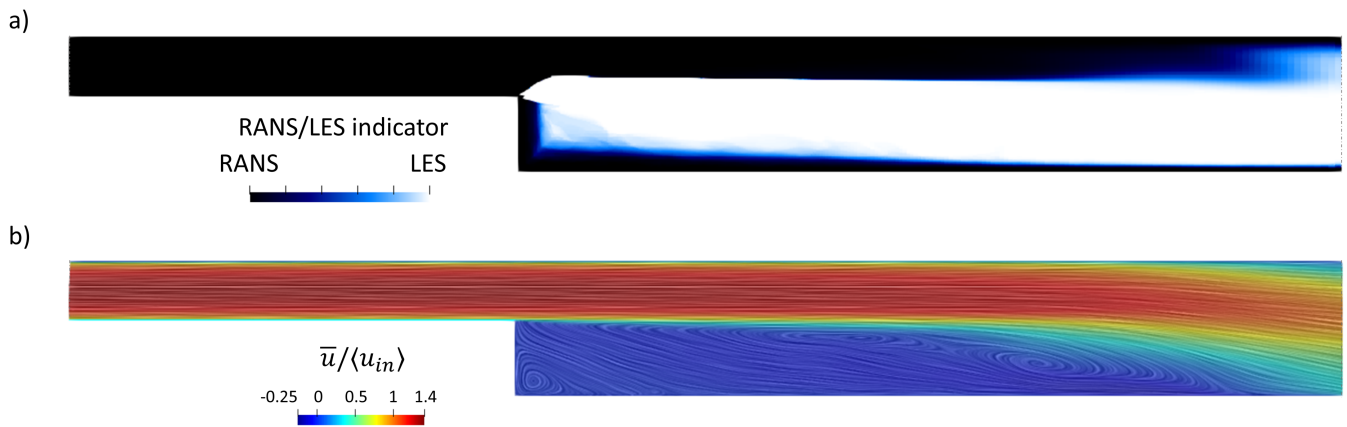


Fig. 14: Midplane side view of DDES simulation. (a) Time-averaged RANS / LES indicator function. White is always LES, black is always RANS, mix is sometimes LES, sometimes RANS. (b) Time-average streamwise velocity  $\bar{u}$ , including in-plane streamlines.

#### 4.2.4 Improved Delayed Detached Eddy Simulations (IDDES)

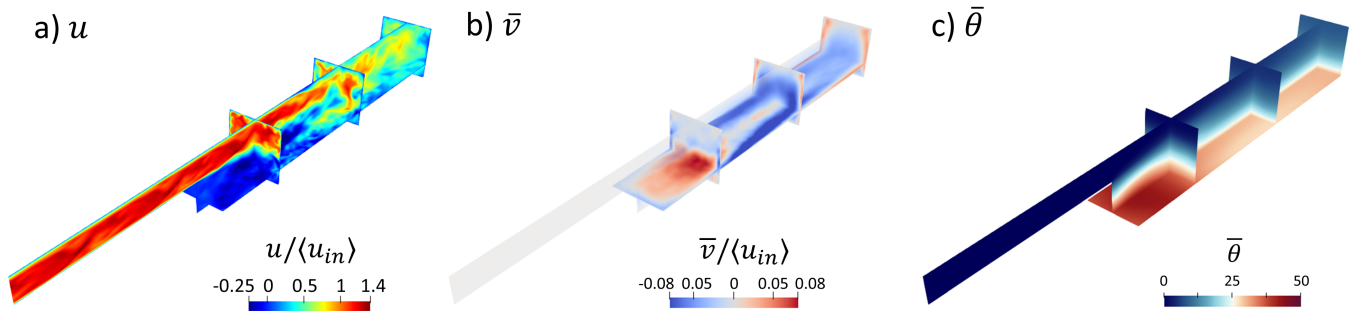


Fig. 15: Flow field visualization for IDDES. a) Streamwise velocity snapshot  $u$ . b) Time-averaged vertical velocity  $\bar{v}$ . c) Time-averaged temperature  $\bar{\theta}$ .

**Qualitative flow field description** As introduced in Sect. 3.2, IDDES was developed as a DDES formulation that would be more amenable to WMLES. Indeed, Fig. 15 shows the flow and temperature fields to be very similar to fields from LES and DES (which was shown to behave as WMLES). Interestingly, the shielding functions do not prohibit LES zones in the upstream channel flow, but do create a peculiar RANS zone immediately adjacent to the step separation point as shown in Fig. 16.

**Midplane profiles** Even though some quantitative differences are apparent, the qualitative behavior of profiles in Fig. 11 further confirms the affinity of IDDES to DES and LES for the current case, both in terms of velocity and turbulence kinetic energy. Further assessment of these quantitative differences and their impact on accuracy is addressed in Sect. 4.3 below.

**Summary** Results presented in the current section highlight that IDDES behaves very similarly to DES, i.e., with an overall WMLES approach throughout the domain. A small difference in RANS / LES zones is observed, but this does not seem to cause a significant difference in flow, temperature, or turbulence profiles at the midplane.

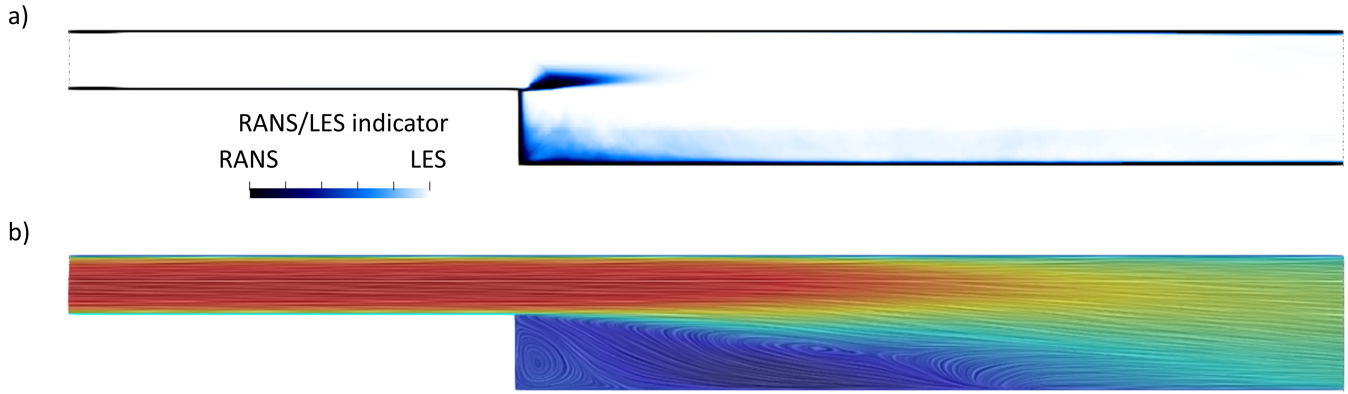


Fig. 16: Midplane side view of IDDES simulation. (a) Time-averaged RANS / LES indicator function. White is always LES, black is always RANS, mix is sometimes LES, sometimes RANS. (b) Time-average streamwise velocity  $\bar{u}$ , including in-plane streamlines.

Tab. 3: Mean absolute error of midplane profiles compared to DNS reference (Oder et al., 2019). Relative MAE values are shown in brackets, and are normalized with mean of DNS profiles. Best and worst values for every variable are indicated in boldfaced and underlined text respectively.

Model	$MAE_{\bar{u}}$	$MAE_{\bar{v}}$	$MAE_{\bar{k}}$	$MAE_{\bar{\theta}}$
RANS	0.092 [7.3%]	0.012 [16.0%]	0.0063 [9.0%]	0.38 [0.9%]
SAS	0.123 [9.7%]	0.011 [15.5%]	0.0063 [8.9%]	0.47 [1.0%]
DES	0.049 [3.9%]	0.009 [12.9%]	0.0051 [7.2%]	0.29 [0.7%]
DDES	<u>0.150 [12%]</u>	<u>0.023 [32.0%]</u>	<u>0.0160 [22.7%]</u>	<u>0.95 [2.2%]</u>
IDDES	0.052 [4.1%]	0.009 [12.2%]	0.0061 [8.7%]	0.44 [1.0%]
LES	<b>0.036 [2.8%]</b>	<b>0.006 [8.8%]</b>	<b>0.00387 [5.5%]</b>	<b>0.25 [0.6%]</b>

### 4.3 Discussion and quantitative performance assessment

In the previous sections, a qualitative discussion and comparison of the flow fields of the considered models was performed. A comparison between steady RANS and LES showed that large-eddy resolution in the SSL allows to significantly improve the overall match with DNS data, justifying that the current BFS setup is suitable for testing the performance of locally scale-resolving hybrid methods. Results obtained from the hybrid simulation indicated that, for the current case, their behavior can be classified in three groups. Firstly, SAS resembles a steady RANS field, with virtually no scale resolution and similar flow field characteristics. Secondly, DES and IDDES behave like WMLES, where the entire domain is simulated as an LES zone, except for regions in the direct wall vicinity. Thirdly, DDES exhibits an interesting hybrid domain subdivision, in which only the SSL is an LES zone, whereas the inlet channel and top wall are predominantly RANS. This latter configuration is promising, as it turns to scale resolution only in the region where RANS clearly struggles to match the DNS data. The different behavior between DDES and IDDES (which are formulated in a relatively similar manner) is an interesting observation, possibly indicating a sensitive bifurcation in the behavior of these methods for this setup.

In the current section, we perform a more quantitative comparison between the several models. Firstly, we compute the mean absolute error (MAE) of midplane profiles from previous sections with the DNS reference data. Next, we expand the performance assessment from midplane values to also include spanwise variation: we quantify observed differences in three-dimensional recirculation structure by computing a spanwise-averaged wall shear stress, and compare integrated mean quantities.

Tab. 3 provides a quantitative comparison of all considered turbulence models based on the MAE of profiles with respect to DNS shown in the discussions above. MAE is averaged over height and over all shown profiles. A first observation is that the temperature  $\bar{\theta}$  is well predicted by all models, whereas the vertical velocity  $\bar{v}$  generally exhibits the largest error. Next, we see that general qualitative observations from previous sections are reaffirmed here, i.e. LES has the lowest MAE overall for every variable, whereas RANS shows significantly larger MAE than LES. SAS does not significantly improve the accuracy in comparison to RANS, while the WMLES-like behavior of DDES and IDDES result in important error reduction, more specifically for  $\bar{u}$  and  $\bar{v}$ . Finally, DDES, even though it shows a promising RANS / LES domain partition, has the poorest accuracy of all simulations, caused by the MSD resulting from a delayed transition of the separated shear layer downstream of the step.

A recurring observation throughout Sect. 4 has been the different structure of both vertical and backflow velocity close to the step, which suggests a different organization of the recirculation and reattachment in the different simulations. To quantify this, we compute the time- and spanwise-averaged wall shear stress  $\bar{\tau}$  at the bottom surface downstream of the step as

$$\bar{\tau}/\rho = \frac{1}{TL_z} \int_0^{L_z} \int_0^T \tau_{\text{wall}}(x, z, t)/\rho \, dt \, dz, \quad (8)$$

which is plotted as a function of streamwise location in Fig. 17. The zero-crossing of  $\bar{\tau}$  represents a spanwise-averaged reattachment point. LES, DES, and IDDES, reaffirm their resemblance and fidelity by closely matching the reattachment point observed in the

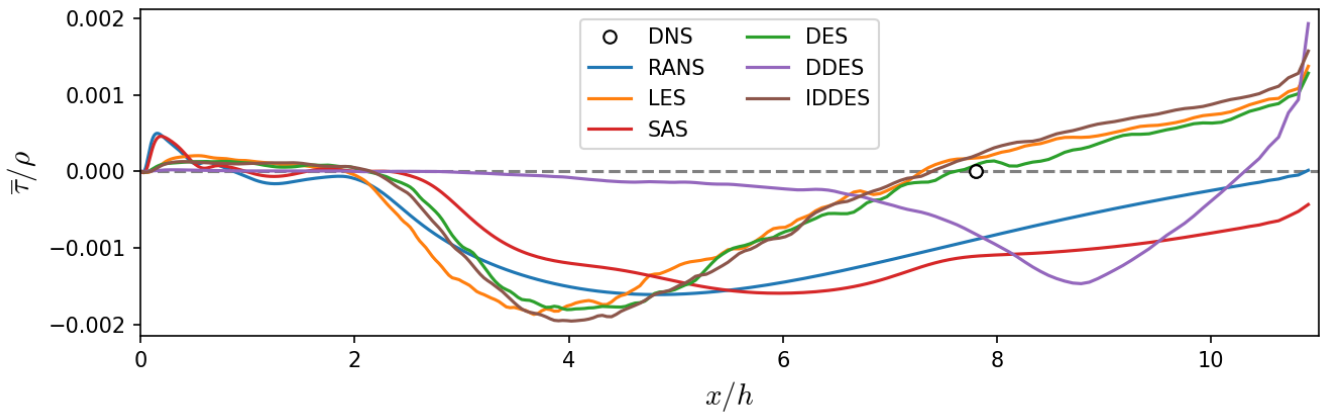


Fig. 17: Time- and spanwise-averaged wall shear stress for RANS, LES, SAS, DES, DDES, and IDDES. DNS reattachment shown with circle.

Tab. 4: Mean outlet temperature and spanwise-integrated reattachment point.

Model	Mean outlet temperature [-]	Spanwise-integrated reattachment point [-]
DNS	12.84	7.81
RANS	13.16 [+2.6%]	10.89 [+39.4%]
SAS	12.00 [-6.5%]	N.A.
DES	13.08 [+1.9%]	7.61 [-2.6%]
DDES	11.37 [-11.4%]	10.32 [+32.3%]
IDDES	13.12 [+2.2%]	7.40 [-5.21%]
LES	13.05 [+1.6%]	7.3 [-6.5%]

reference DNS. Also, RANS and SAS are both shown to severely overpredict the size of the recirculation bubble, with RANS reattaching at  $x/h \approx 11$ , and SAS not reattaching at all. DDES finally shows a different recirculation structure from any of the other models, caused by the MSD mentioned above.

Tab. 4 shows a summary of mean integrated quantities for the reference DNS data and all models considered in the current report. More specifically, the table contains the mean outlet temperature and the spanwise-integrated reattachment point (based on the zero crossing in Fig. 17). Firstly, the table shows that the mean outlet temperature is generally well predicted, although SAS and DDES perform significantly worse than the other models. Furthermore, as expected from Fig. 26, the spanwise-reattachment point shows a significant dichotomy between DES, IDDES, and LES on the one hand, which match DNS data fairly well, and RANS, SAS, and DDES on the other, each of which mispredicts the reattachment with relative errors well over 30%.

## 5 Sensitivity studies

An important note to make on the results presented in the previous section is they are all performed on a fine mesh suitable for highly-resolved LES, as shown by the minor contribution of sub-grid LES terms in Fig. 5. Therefore, the computational cost of all simulations (except for the steady RANS) is roughly equal. However, an appeal of hybrid and RANS methods is that they potentially retain their accuracy on more affordable meshes, since RANS zones are more robust to coarse resolutions than LES. For this reason, we present a grid study here below in Sect. 5.1, and quantify error sensitivity of different turbulence models to grid coarsening. Furthermore, it was already noted that, even though DDES produces a generally favorable RANS / LES domain partitioning, the late development of resolved turbulence causes severe MSD, which is potentially an artefact of the relatively low Reynolds number of the current test case. Therefore, we perform a Reynolds-number sensitivity study of DDES in Sect. 5.2.

### 5.1 Grid resolution sensitivity

The study is performed with 6 coarsened grids (C1 – C6), where the baseline grid resolution is sequentially reduced by 20% in all spatial directions, resulting in an overall reduction of degrees of freedom by a factor about 2 per coarsening step, or a total reduction of about 160 over the entire range.

A first observation from Tab. 5 (top) is the insensitivity of RANS error to the grid resolution over the large range of coarsening. On the other side of the spectrum, we see that LES shows a monotonous decrease in accuracy with grid coarsening, as fewer turbulent scales can be resolved by the grid and have to be accounted for by the sub-grid scale model. The crossover point, where RANS attains similar or superior accuracy over LES, lies around a resolution between the C3 grid and C4 grid. It was found that, around this point, the domain-integrated fraction of resolved to total turbulent kinetic energy in LES is about 80% for these grids, corresponding with the general 80% rule-of-thumb for a proper LES. These are promising observations especially for the LES-like hybrid methods DES, DDES and IDDES, as grid coarsening could convert LES zones to RANS zones, and it is observed that in RANS zones the grid resolution, and hence the computational cost, can be significantly reduced without sacrificing accuracy.

Tab. 5: Top: *Averaged error metric* for sensitivity study including baseline (B) and coarsened grids (C1 – C6). Degrees of freedom per grid are shown in parenthesis. Best and worst errors for every grid indicated in boldfaced and underlined text respectively. Bottom: *Domain LES fraction* for DES, DDES, and IDDES. Boldfaced text indicates configuration with RANS at inlet and walls combined with LES in SSL

	B	C1	C2	C3	C4	C5	C6
<i>Averaged error metric</i>	(3.7M)	(1.9M)	(942k)	(465k)	(230k)	(106k)	(52k)
RANS	9.6%	9.8%	9.9%	9.8%	<b>9.9%</b>	<b>9.5%</b>	<b>9.5%</b>
SAS	10.4%	10.8%	11.2%	11.3%	10.3%	9.9%	9.9%
DES	7.3%	10.8%	23.0%	<u>21.9%</u>	<u>21.3%</u>	<u>20.9%</u>	<u>19.1%</u>
DDES	<u>20.1%</u>	<u>18.3%</u>	<u>21.9%</u>	17.4%	18.0%	18.0%	17.6%
IDDES	8.0%	10.4%	12.0%	11.7%	15.9%	16.6%	14.6%
LES	<b>6.2%</b>	<b>8.2%</b>	<b>8.7%</b>	<b>9.5%</b>	11.5%	12.4%	13.3%
<i>Domain LES fraction</i>	B	C1	C2	C3	C4	C5	C6
DES	87%	86%	56%	57%	57%	61%	67%
DDES	<b>41%</b>	<b>38%</b>	56%	<b>31%</b>	<b>30%</b>	<b>31%</b>	<b>27%</b>
IDDES	88%	87%	85%	<b>33%</b>	<b>36%</b>	<b>34%</b>	<b>26%</b>

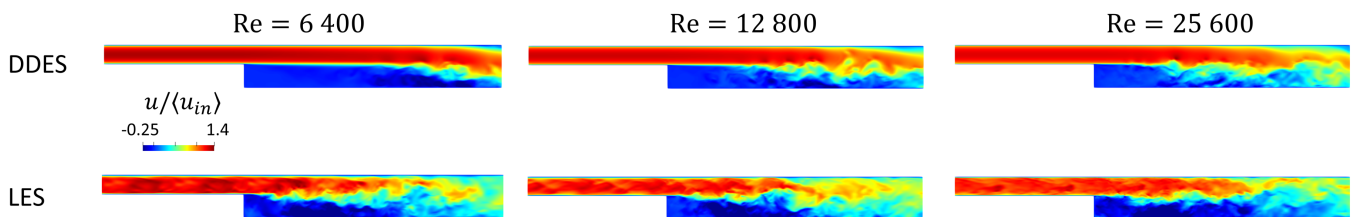


Fig. 18: Snapshots of streamwise velocity for  $Re = 6400, 12800, 25600$  for DDES (top) and LES (bottom).

However, investigation of the hybrid performance shows that this promise remains unfulfilled, as none of the hybrid methods can retain accuracy higher than the RANS baseline error of 9.6% upon grid coarsening. DDES remains very poor for all grids considered. DES exhibits a sharp error increase for grid C2. Further investigation showed this was caused by a laminarization of the inlet channel in LES mode. Indeed, Tab. 5 (bottom) shows that DES retains its WMLES character and does not switch to RANS zones, even at the coarsest grids. IDDES shows a gradual increase in errors due to a switch towards the configuration with RANS at inlet and walls, and LES in the SSL. However, in this mode IDDES suffers from MSD, resulting in large errors. The observations in the current section allow to draw important conclusions regarding the hybrid methods considered in this report for the current low-Reynolds number BFS flow. Although for LES-suited grids DES and IDDES improve the match with DNS data compared to the baseline RANS by running in WMLES mode, these improvements are not retained upon grid coarsening. SAS and DDES never succeed to surpass RANS accuracy. A further interesting finding is that, for each grid resolution, the best setup is either RANS or LES, but never a hybrid turbulence model setup. Note that some of these findings are potentially linked to the low Reynolds number of the current setup. For this reason, a Reynolds-number sensitivity study is performed in the next section.

## 5.2 Reynolds-number sensitivity of DDES

The previous sections have shown that, in some configurations, DDES and IDDES automatically assign only the separated shear layer a LES treatment while the rest of the domain remains in RANS mode. In principle, this is a highly desirable configuration, but the simulations show strong MSD effects, in which there is a lack of resolved turbulence in the SSL to fill in for the absence of a RANS turbulence model.

It was noted that this lack is possibly caused by the relatively low Reynolds number of the considered problem, and that a higher Reynolds number could result in much earlier natural transition of the LES shear layer and thus better performance of the hybrid methods. Therefore, in the current section, we investigate the BFS at doubled and quadrupled Reynolds numbers, i.e. at  $Re = 6400$  and  $Re = 12800$ , respectively. Since there is no DNS data available for these cases, and running additional DNS is outside of the scope of the current work, we use the LES as a high-fidelity reference for comparison with DDES. The LES and DDES are run using the baseline grid, resulting in a slightly lower effective resolution considering these increased Reynolds numbers. The RANS/LES zones of the considered DDES were confirmed to be in the configuration where only the SSL is in LES mode. Snapshots of DDES and LES streamwise velocities  $u$  are shown in Fig. 18 for all three Reynolds numbers. The LES (bottom panels) expectedly shows smaller turbulence scales at the higher Reynolds numbers, although the overall flow field features seem similar. The DDES on the other hand does show an important acceleration of the transition to scale resolution in the SSL. This is further confirmed by the visualization of total (resolved + modeled) turbulent kinetic energy  $\bar{k}$  in Fig. 19. While LES shows a coherent region of high  $\bar{k}$  in the SSL directly following the step that seems insensitive to the Reynolds number, the point of onset clearly advances towards the step with increasing Reynolds number in the DDES solution. However, even though transition is accelerated, the zone directly adjacent to the step remains turbulence-deficient, indicating possible MSD even at higher Reynolds numbers. Also, the  $Q$ -criterion isosurfaces in Fig. 20 show that, even at the highest Reynolds number, DDES scale development is still slightly delayed compared to LES, which features vortex resolution throughout the entire domain.

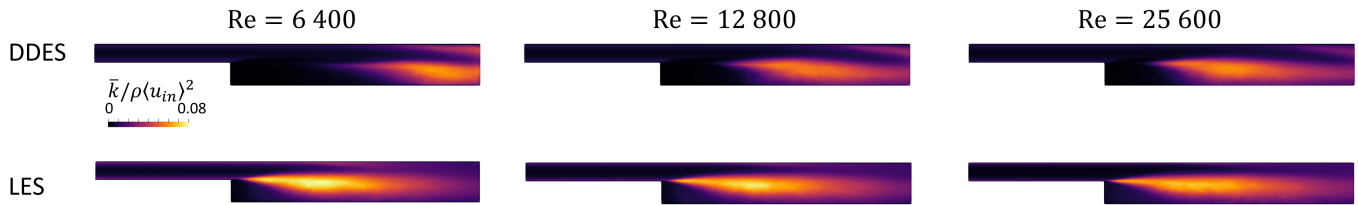


Fig. 19: Time-averaged total (modeled + resolved) turbulent kinetic energy for  $Re = 6400, 12800, 25600$  for DDES (top) and LES (bottom).

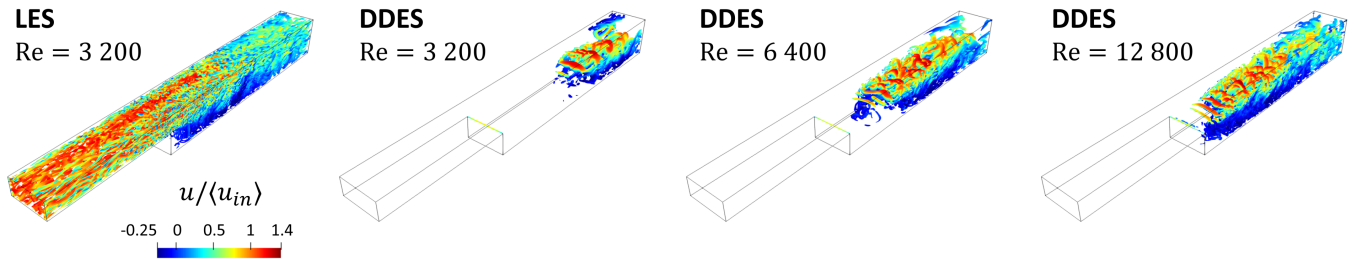


Fig. 20: Isosurfaces of vortex identification  $Q$  criterion (second invariant of velocity gradient tensor for LES at baseline  $Re$  and DDES at baseline+increased  $Re$ ). The  $Q$  isovalue is 100, and coloring is by instantaneous streamwise velocity  $u$

Indeed, when comparing profiles of time-average streamwise and vertical velocities in Fig. 21 it is shown that, while the accelerated transition causes the strongly negative vertical velocity zones to occur closer to the step at higher Reynolds number (i.e. starting from  $x/h = 5$ ), the match between DDES and the reference data (LES in this case), is still very poor. Furthermore, the streamwise velocity still shows negligible recirculation for  $0 \leq x/h \leq 5$ . In contrast, the LES seems relatively insensitive to the increase in Reynolds number based on the current qualitative investigation.

We conclude from this sensitivity study that, at higher  $Re$ , scale development in the SSL LES zones of the hybrid DDES is accelerated, although for current simulations, it is still lagging behind significantly compared to LES, resulting in a poor match between LES and DDES. Further investigations should be performed on whether promoting transition is possible by more advanced hybrid methods, perhaps including stochastic seeding near the step, or whether the early development observed in LES can only be triggered by bypass-type transition induced by resolved fluctuations coming from the channel.

## 6 Conclusion

We have investigated hybrid turbulence models for a confined BFS flow at low Prandtl number and relatively low Reynolds number. Simulations were performed using RANS, LES, and hybrid SAS and DES variants. Results were compared to existing high-fidelity DNS data. A first set of simulations was performed on a fine simulation grid with 3.7 million cells. A comparison between RANS and LES showed that partial scale resolution allows to significantly improve the overall match with DNS, justifying the current BFS setup is suitable for testing the performance of locally scale-resolving hybrid methods. Results obtained from the hybrid simulations indicate that, for the current case, their behavior can be classified in three groups. Firstly, SAS resembles a steady RANS field, with virtually no scale resolution and similar flow field characteristics. Secondly, DES and IDDES behave as WMLES, where the entire domain is simulated as an LES zone, except for regions in the direct vicinity of the wall. Thirdly, DDES exhibits a more classical hybrid domain partitioning, in which only the SSL is an LES zone, whereas the inlet channel and top wall are predominantly RANS. This latter configuration is promising, as it turns to scale resolution only in the region where RANS clearly struggles to match the DNS data.

A quantitative comparison revealed that, while temperature profiles are predicted generally well for all models due to the low Prandtl number, the (WM)LES type models DES and IDDES emerge as the higher-fidelity hybrid turbulence models, outperform RANS and approximating LES accuracy. In contrast, SAS and DDES fail to consistently improve over RANS. Especially the recirculation structure and associated reattachment point are very ill-predicted by the SAS and DDES, whereas DES and IDDES closely adhere to the LES and DNS. While SAS does not qualitatively distinguish itself from RANS, the DDES suffers from MSD caused by a lack of resolved turbulence in the LES zone close to the step, where the mixing support of a RANS turbulence model has already vanished.

A grid coarsening study was performed to quantify the error degradation of all models, as well as the switching behavior between RANS and LES zones for DES and its variants. The grid study showed that, although its error metrics continuously worsen with coarsening, LES retains superior accuracy over RANS except for very coarse grids. However, none of the hybrid methods retained their improvements over RANS for coarsened grids. Further, the best-performing model for each grid was either RANS or LES, never a hybrid turbulence model.

Given the low Reynolds number of the current setup, we further investigated the effect of the Reynolds number on the failure to early transition the SSL with resolved turbulence in the configuration with LES only in the SSL region. Additional LES and DDES for the baseline grid were performed for two higher Reynolds number increased with a factor 2 and 4 respectively. Although time-averaged LES flow features appear relatively insensitive to this increase, the DDES clearly shows earlier transition at the

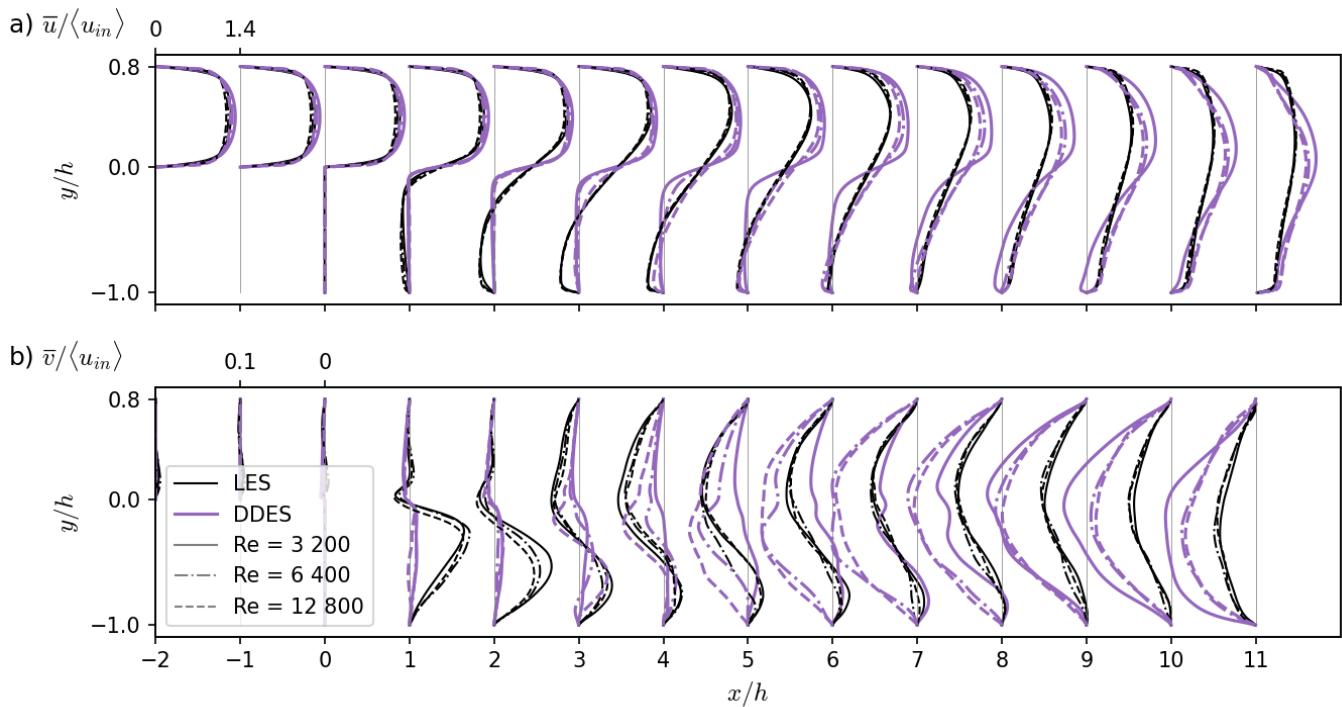


Fig. 21: Profiles along midplane of time-averaged velocity for LES and DDES at three different Reynolds numbers. (a) Streamwise velocity component  $\bar{u}$ . (b) Vertical velocity component  $\bar{v}$ .

higher Reynolds numbers, even though lack of resolved turbulence in the immediate vicinity of the step results in an unsatisfactory comparison to the LES data.

In conclusion, it was shown that, for the current setup, the considered hybrid methods only perform adequately if the grid allows them to run in WMLES mode throughout the entire domain, and that attempts to reduce computational cost with regard to a full LES invariably lead to a strong increase in error for the hybrid models. However, also more promising observations were made, mainly that DDES and IDDES are capable of automatically dividing the domain into desirable RANS and LES zones, and that higher Reynolds numbers appear to promote scale development closer to the step.

We close with suggestions for future research. A similar investigation for significantly higher Reynolds numbers will clarify whether current models automatically improve by earlier natural scale development. Also, it would be interesting to see whether scale development is promoted by perturbations close to the separation point, or whether such immediate development can only be attained by resolved turbulence in the channel, which triggers a bypass-type transition in the SSL. Finally, it is important to note that we only considered ready-to-use standard hybrid techniques available in OpenFOAM v2012. It would be interesting to further assess the behavior of more advanced hybrid models that promise rapid transition in separated flows for the current BFS setup (Shur et al., 2015).

## Acknowledgements

The authors thank dr. Jure Oder and Matilde Fiore for fruitful discussions. This work has been performed in context of the PATRICIA project, which has received funding from European Union's Horizon 2020 Research and Innovation programme under grant agreement No. 945077.

## References

- N. Ashton, A. West, S. Lardeau, and A. Revell. Assessment of RANS and DES methods for realistic automotive models. *Computers & Fluids*, 128:1–15, 2016.
- Y. Bartosiewicz and M. Duponcheel. Large-eddy simulation: Application to liquid metal fluid flow and heat transfer. In *Thermal Hydraulics Aspects of Liquid Metal Cooled Nuclear Reactors*, pages 245–271. Woodhead Publishing, 2019. ISBN 978-0-08-101980-1.
- S. Bhushan, M. Elmellouki, T. Jamal, G. Busco, D.K. Walters, Y.A. Hassan, E. Merzari, and A. Obabko. Assessment of low-and high-fidelity turbulence models for heat transfer predictions in low-Prandtl number flows. *Nuclear Engineering and Design*, 388: 111614, 2022.
- B. Chaouat. The state of the art of hybrid RANS/LES modeling for the simulation of turbulent flows. *Flow, Turbulence and Combustion*, 99(2):279–327, 2017.
- Y. Egorov and F.R. Menter. Development and application of SST-SAS turbulence model in the DESIDER project. In *Advances in Hybrid RANS-LES Modelling*, pages 261–270. Springer, 2008.

- A. Frendi, A. Tosh, and S. Girimaji. Flow past a backward-facing step: comparison of PANS, DES and URANS results with experiments. *International Journal for Computational Methods in Engineering Science and Mechanics*, 8(1):23–38, 2006.
- M.S. Gritskevich, A.V. Garbaruk, J. Schütze, and F.R. Menter. Development of DDES and IDDES formulations for the  $k-\omega$  shear stress transport model. *Flow, Turbulence and Combustion*, 88(3):431–449, 2012.
- W. Haase, M. Braza, and A. Revell. *DESider—A European Effort on Hybrid RANS-LES Modelling: Results of the European-Union Funded Project, 2004-2007*, volume 103. Springer Science & Business Media, 2009.
- W. Kim and S. Menon. A new dynamic one-equation subgrid-scale model for large eddy simulations. In *33rd Aerospace Sciences Meeting and Exhibit*, page 356, 1995.
- L. Koloszar and V. Moreau. (U)RANS pool thermal hydraulics. In *Thermal Hydraulics Aspects of Liquid Metal Cooled Nuclear Reactors*, pages 341–359. Elsevier, 2019.
- F.S. Lien and M.A. Leschziner. Assessment of turbulence-transport models including non-linear RNG eddy-viscosity formulation and second-moment closure for flow over a backward-facing step. *Computers & Fluids*, 23(8):983–1004, 1994. ISSN 0045-7930.
- F.R. Menter, M. Kuntz, and R. Langtry. Ten years of industrial experience with the SST turbulence model. *Turbulence, Heat and Mass Transfer*, 4(1):625–632, 2003.
- F.R. Menter, A. Hüppe, A. Matyushenko, and D.M. Kolmogorov. An overview of hybrid RANS–LES models developed for industrial CFD. *Applied Sciences*, 11(6):2459, 2021.
- P. Moin and K. Mahesh. Direct numerical simulation: a tool in turbulence research. *Annual Review of Fluid Mechanics*, 30(1): 539–578, 1998.
- J. Oder, A. Shams, L. Cizelj, and I. Tiselj. Direct numerical simulation of low-Prandtl fluid flow over a confined backward facing step. *International Journal of Heat and Mass Transfer*, 142:118436, 2019.
- A. Probst, C. Wolf, R. Radespiel, T. Knopp, D. Schwamborn, and R. Radespiel. A comparison of detached-eddy simulation and Reynolds-stress modeling applied to the flow over a backward-facing step and an airfoil at stall. In *48th AIAA aerospace sciences meeting including the New horizons forum and aerospace exposition*, page 920, 2010.
- F. Roelofs, P. Planquart, and L. Koloszar. Best practice guidelines for nuclear liquid metal CFD. In *Thermal Hydraulics Aspects of Liquid Metal Cooled Nuclear Reactors*, pages 407–419. Elsevier, 2019.
- P. Sagaut. *Large eddy simulation for incompressible flows: an introduction*. Springer Science & Business Media, 2006.
- M.L. Shur, P.R. Spalart, M.K. Strelets, and A.K. Travin. An enhanced version of DES with rapid transition from RANS to LES in separated flows. *Flow, Turbulence and Combustion*, 95(4):709–737, 2015.
- J.P. Slotnick, A. Khodadoust, J. Alonso, D. Darmofal, W. Gropp, E. Lurie, and D.J. Mavriplis. CFD vision 2030 study: a path to revolutionary computational aerosciences. Technical report, 2014.
- E.M. Smirnov, A.A. Smirnovsky, N.A. Schur, D.K. Zaitsev, and P.E. Smirnov. Comparison of RANS and IDDES solutions for turbulent flow and heat transfer past a backward-facing step. *Heat and Mass Transfer*, 54(8):2231–2241, 2018.
- P.R. Spalart. Detached-eddy simulation. *Annual Review of Fluid Mechanics*, 41:181–202, 2009.
- M Strelets. Detached eddy simulation of massively separated flows. In *39th Aerospace sciences meeting and exhibit*, page 879, 2001.
- I. Tiselj and J. Oder. Direct numerical simulation of a backward-facing step. In *Technical Deliverable of Euratom RIA SESAME project*. 2019.
- H. G. Weller, G. Tabor, H. Jasak, and C. Fureby. A tensorial approach to computational continuum mechanics using object-oriented techniques. *Computers in Physics*, 12(6):620–631, 1998.